Hindawi
Advances in Civil Engineering
Volume 2023, Article ID 9246508, 14 pages
https://doi.org/10.1155/2023/9246508

Research Article

Analysis of *U*-Shaped Steel Failure Characteristics in Rock Burst Roadway and Design of Stable Structure and Constant Resistance *O*-Shed

Lianman Xu,[1] **Jinzhu Zhang**,[1] **Rixin Guo**,[1] **Tianhao Li**,[1] **Zhijiao Qin**,[1] **Aiwen Wang**,[2] **Jiquan Sheng**,[3] **Yonghui Xiao**,[4] **Jianqiang Chen**,[5] **and Kunlun Liu**[5]

[1]*School of Environment, Liaoning University, Shenyang, Liaoning 110036, China*
[2]*School of Mechanics and Engineering, Liaoning Technical University, Fuxin, China*
[3]*Laohutai Coal Mine, Fushun Minel Industry (Group) Co. Ltd., Fushun, China*
[4]*School of Physics, Liaoning University, Shenyang, China*
[5]*Shenhua Xinjiang Energy Co. Ltd., Xinjiang, China*

Correspondence should be addressed to Lianman Xu; xulianman@lnu.edu.cn

Received 14 October 2022; Accepted 5 December 2022; Published 9 January 2023

Academic Editor: Ma Jianjun

The *U*-shaped steel support has good surface protection and is one of the main supporting forms of the roadway under rock bursts. However, in the supporting process of roadways under rock burst, there are poor mechanical properties of lap joints, resulting in a serious decline in the anti-impact performance of *U*-shaped steel supports. Using a combination of laboratory experiments and theoretical analysis, we study the sliding mechanism of the *U*-shaped steel bracket's overlap section bearing and find the key factors affecting the sliding performance of the overlap section. The characteristics of deformation and failure of *U*-shaped steel supports under impact loads are analyzed by numerical calculations. An improved method for optimizing the sliding performance of the lap section is proposed to provide theoretical support for the design of stable and constant-resistance energy-absorbing *O*-shed supports. The research results show that the frictional properties between the contact surfaces of the overlapped sections, especially the frictional properties between the contact surfaces of the clamp and the *U*-shaped steel, determine the sliding characteristics of the *U*-shaped steel overlapped sections, which are the key factors affecting the bearing capacity of the support. The single-point maximum bearing capacity of the *U*-shaped steel bracket under the uniformly distributed impact load is basically close to the maximum bearing capacity of the *U*-shaped steel bracket under the concentrated impact load. When the *U*-shaped steel bracket is uniformly loaded, its bearing capacity can be increased several times. When a gasket is added between the *U*-section steel and the clamping bolt in the lap section, the bearing capacity changes smoothly during the sliding process, which greatly improves the friction performance between the contact surfaces, and can greatly improve the overall bearing capacity, energy absorption, and anti-impact performance of the support structure. Based on this, a stable and constant energy-absorption *O*-type shed structure for the impacted underground roadway in Laohutai Mine was proposed. The field application proved that improving the sliding performance at the joint of the *U*-shaped steel support can effectively control the deformation of the roadway under the impact load.

1. Introduction

U-shaped steel supports can maintain the stability of roadways with broken surrounding rocks and have good surface protection. In particular, the closed *U*-shaped steel and the interframe tie rod constitute a "cage" support structure, which is one of the main support forms of a rock burst roadway [1–6]. Along with our country entering the stage of deep mining in coal mines, the roadway surrounding rock underwent high stress and a strong impact load; the more serious rock bursts occurred in a single bolt anchor cable, producing the phenomenon of serious fall-off

bolt failure and being unable to maintain the stability of the coal or rock roadway surface, causing a severe roadway crowd break accident [7–9]. When strong earthquakes occur frequently in deep mines, it will bring great hidden dangers to mine safety production. The location of high-energy mining seismic release does not match the location of microseismic accumulation, and the structural occlusion instability will occur in the process of rock fracture [10]. *U*-shaped steel supports can control the displacement and deformation of surrounding rock on the roadway under impact loads, avoid the outburst of a large number of coal and rock fragments, prevent the occurrence of disastrous rock burst accidents, and have great significance for improving the stability and safety of rock burst roadways [11–13].

The *U*-shaped steel support is a kind of roadway support with mature technology. After nearly 90 years of development, scholars at home and abroad have carried out a lot of studies on the existing problems of *U*-shaped steel support and put forward many improvement measures, such as the fact that the supporting performance of *U*-shaped steel support can be effectively improved by adding prestressed anchor cable, structural compensation for weak links of support, back-wall filling or back-wall grouting, and leg-lock support for dangerous section positions [14–20]. Through numerical simulation and field industrial experiments, Xie et al. proposed to increase the bearing capacity and anti-deformation capacity of *U*-shaped steel supports through the anchoring of anchor cables, so as to realize the overall bearing capacity of *U*-shaped steel supports [15]. Liang et al. established a rock dynamic boundary surface plastic damage model considering high strain, which was used to capture the dynamic characteristics of the stress on *U*-shaped steel supports. At the same time, the thermoelastoplastic coupled damage model of concrete under dynamic load is established, a more general shock load equation of state (GEOS) is used to represent the strain-average pressure, and the micromechanical constitutive model parameters of the four-dimensional spring model (4D-LSM) are determined. It is applied to simulate and analyze the instantaneous deformation failure of *U*-shaped steel under different initial impact velocities [16–18]. Wang et al. established a mechanical model of the *U*-shaped steel support and surrounding rock-bearing capacity and proposed the reinforcement support method of anchor cable with a longitudinal steel belt beam in the middle of the shed leg, shoulder socket, and middle of the arch beam [20]. Jiao et al. analyzed the failure mechanism and stability effect of segment lining through field monitoring, numerical simulation, and the numerical analysis method of rock and soil mechanics. In rock engineering, the damage evolution under load has an important influence on the stiffness and deformation characteristics of rock mass [22, 23]. Jiao et al.improved the traditional *U*-shaped steel structures and improved the supporting effect of *U*-shaped steel supports in loose thick coal seams [21]. Ma et al. believed that adding leg bolts and pressure relief drilling could effectively improve the supporting effect of the *U*-shaped steel support [24]. You Chunan et al. discussed the influence of cable pretightening force on the shrinkage resistance of *U*-shaped steel retractable supports and showed that, under certain conditions, different cable pretightening forces could be applied to obtain different shrinkage resistance to meet the design requirements [25]. Ma et al. proposed an anisotropic plastic model to describe the nonisotropic mechanical behavior of porous media and established the model under the critical state framework using the boundary surface plasticity theory [26]. Chen et al. established the calculation model of cracking load and peak load of the UHPC-NC structure and considered the influences of UHPC's high tensile strength, NC rebar, UHPC rebar, and UHPC prestressed reinforcement on cracking load and peak load so as to provide a reference for the range of tensile strength of *U*-shaped steel support materials [27]. *U* steel support in bolting technology and supporting continuous improvement methods, a substantial increase in support of *U*-shape set performance, but in recent years, since the deep roadway impact ground pressure hazard in the roadway in deep shock pressure often *U*-shape set a serious damage, such as stents has not given full play to the bearing capacity and working resistance under impact load drastically reduced. Uneven backfilling of the support wall leads to buckling deformation and distortion deformation of the support, and the overall bearing capacity of the support cannot be exerted [28–30].

For the deep roadway *u*-shape impact ground pressure damage phenomenon, the experimental study on the friction properties of the *U*-shaped steel lap section during the sliding process was carried out by combining laboratory experiments and theoretical analysis, and the sliding mechanism of the *U*-shaped steel bracket lap section and the friction properties of the contact surface were obtained. The deformation and failure laws of the *U*-shaped steel bracket under the impact load were studied by numerical simulation. Finally, the failure characteristics of *U*-shaped steel support in deep rock burst roadway are obtained, and combined with the failure characteristics analysis of *U*-shaped steel in rock burst roadway, the *O*-shaped shed structure with a stable structure and constant resistance and energy absorption of rock burst roadway in Hutai Mine is proposed. The field application proves that improving the sliding performance of *U*-shaped steel support joints can effectively control the deformation of the roadway under the impact load. Based on this, a method to optimize the bearing performance of the *U*-shaped steel bracket is proposed to provide theoretical and technical support for the design of the stable structure of the *O*-shaped shed bracket with constant resistance and energy absorption.

2. Sliding Friction Mechanism Analysis of a *U*-Section Steel Lap Section

The shrinkage performance and support resistance of the *U*-shaped steel support mainly depend on the pretightening force, clamping type, and clamping force [31, 32]. A large number of studies believe that the shrinkage performance of *U*-section steel is affected by axial force, bending moment, and shear force together [33]. The shrinkage performance of *U*-section steel supports is greatly improved by optimizing

the positioning mode and lap length of the section steel. However, the influence of friction between the contact surfaces in the lap section on the sliding performance and bearing capacity of the *U*-shaped steel is not considered in the abovementioned studies. This paper focuses on the sliding friction mechanism of the lap section of the *U*-shaped steel support and analyzes the influence of the friction performance between lap sections on the shrinkage performance and support resistance of the *U*-shaped steel support, so as to provide a basis for the design and optimization of a stable and constant resistance *O*-type shed.

2.1. Experimental Study on Friction Performance of Lap Segment during Sliding. In the experiment, two sections of 36-*U*-section steel with a length of 500 mm and a lap length of 30 mm were selected. Two-bolt splint clamps were set and placed in the middle of the upper and lower platen of the pressure testing machine. The experimental device is shown in Figure 1, with the pretightening torque of clamps at 250 Nm and the loading speed at 0.4 m/s.

The axial load-displacement curve of the *U*-section lap section is shown in Figure 2. It can be seen from the figure that the axial load-displacement curves of the three groups of lap segments under the same conditions are basically similar. In the initial stage, the relative sliding displacement between the two sections of *U*-shaped steel is very small, and the axial bearing capacity rapidly increases to about 100 kN. As the testing machine continues to load, a large relative sliding displacement begins to occur between two sections of *U*-shaped steel. When the relative displacement between two sections of *U*-shaped steel reaches about 30 mm, the axial bearing capacity reaches its maximum value, and the maximum value of the axial bearing capacity is about 160 kN. When the load on the testing machine exceeds the axial bearing capacity limit, the bearing capacity instantly decreases to less than 100 kN. At this time, there is instantaneous relative sliding between the bolt and *U*-section steel, and the clamp restores to the initial pretightening position from the inclined state, as shown in Figure 3. After the first sudden drop in bearing capacity, the bearing capacity increases sharply at first, then slowly, and when the axial bearing capacity reaches the limit value again, the bearing capacity drops suddenly again. After that, in the loading process, the bearing capacity repeats the periodic fluctuation process of sharp growth, slow growth, and sudden drop. After 2–4 fluctuations, the maximum value of the bearing capacity is reduced to about 100 kN. At this time, the preloading forces of the clamping force decreases seriously, and even the preloading force of the clamping force completely fails.

The internal force change of bolts when *U*-shaped steel is in direct contact with the contact surface of the clamp is shown in Figure 4. After the pretightening of the lap section of *U*-shaped steel, the pretightening force of the bolt at the 3 measuring points from 1# to 3# is 78 MPa, 80 MPa, and 82 MPa, respectively. In the process of loading, the bearing capacity rises rapidly in the initial stage, and the internal force of bolts at three measuring points increases, but the

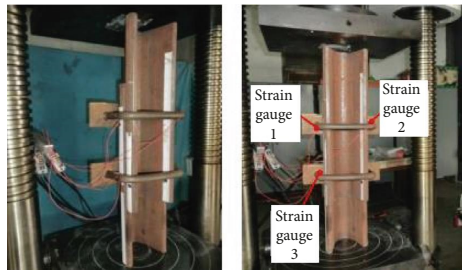

Figure 1: *U*-shape steel axial bearing capacity test device.

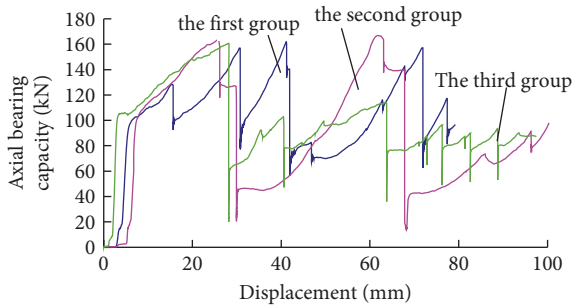

Figure 2: *U*-shape lap section of the axial bearing capacity of the force-displacement relation curve.

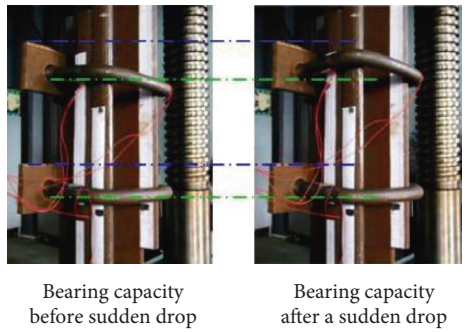

Figure 3: The deformation of the truck before and after the bearing capacity drop.

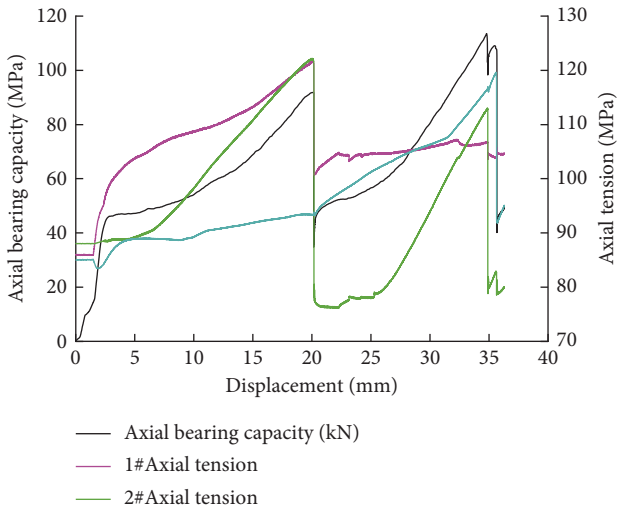

Figure 4: The change in the curve of internal force of bolt in direct contact.

increase is small. When the axial bearing capacity exceeds 45 kN, the relative sliding between the two *U*-shaped steels begins, and the internal force of the bolts at the measuring points $1^{\#}$ and $2^{\#}$ of the upper clamp increases rapidly while the internal force of the bolts at the measuring point $3^{\#}$ of the lower clamp increases little and the upper clamp tilts seriously. Therefore, the bearing capacity is mainly provided by the force between the upper clamp and the *U*-shaped steel. When the axial bearing capacity reaches 90 kN, after the first sudden drop in bearing capacity, the bolt internal force of the measuring points $1^{\#}$ and $2^{\#}$ of the upper clamp also experiences a sudden drop at this moment, but the bolt internal force of the measuring point $3^{\#}$ of the lower clamp has no change. After the bearing capacity drops for the first time, the axial bearing capacity rises again when the load continues. In this process, the internal force of the bolt at measuring point $3^{\#}$ of the lower clamp increases rapidly with the increase in bearing capacity, and the internal force of the bolt at measuring points $1^{\#}$ and $2^{\#}$ of the upper clamp also increases, but its value is far less than the internal force of the bolt at measuring point $3^{\#}$. When the axial bearing capacity reaches 118 kN, the axial bearing capacity has a small sudden drop, and the tensile force of bolts at measuring points $1^{\#}$ and $2^{\#}$ also has a small sudden drop, while the internal force of bolts at measuring point $3^{\#}$ has no obvious change. When the sliding displacement reaches 36 mm, the axial bearing capacity drops again. At this time, the internal forces of bolts at the three measuring points on the upper and lower clamps all drop significantly, and the upper clamps fail to fall.

2.2. Theoretical Analysis of Friction Force and Internal Force Change in Lap Section

2.2.1. Model Building. To analyze the relationship between the clamping preload, friction between the contact surface, and the axial bearing capacity in the sliding process of the lap section, a simplified mechanical model of the lap section of *U*-shaped steel is established. Since the section of *U*-shaped steel is a structural symmetry, half of it is taken for analysis and research. The simplified calculation model is shown in Figure 5, where *U*1 and *U*2 are *U*-shaped steel, and *L*3 and *L*4 are *U*-shaped steel clamping bolts. *B*5 and *B*6 are *u*-shaped steel clamping splints. The static friction coefficient between *U*-section steel and bolts is $\mu 1$, and the dynamic friction coefficient is $\mu 1$.' "The static friction coefficient between *U*-section steel and *U*-section steel is $\mu 2$, and the dynamic friction coefficient is $\mu 2$." The axial pressure exerted by external load on the lap section is *P* and the model is 1/2 model. In the sliding process of *U*-section steel, the clamp tilts and deforms, during which an additional bending moment *M* is generated. The acting force between the components of the lap section mainly includes the acting force of the clamp on the *U*-shaped steel.

After the bolt is pretightened, including *F*31, *F*41, *F*52, and *F*62, strain gauge 1, strain gauge 2, and strain gauge 3 before the bearing capacity drop, 123 axial bearing capacity of the *U*-shaped steel on the clamp, including *F*13, *F*14, *F*25, and *F*26. A pair of interaction forces *F*12 and *F*21 between *U*1 and *U*2, and two pairs of interaction forces *F*35 and *F*53, *F*46 and *F*64 between bolt and splint after pretightening. In the sliding process of *U*-shaped steel, there are also two pairs of interaction friction between *U*1 and the bolts *f*13 and *F*31, *F*14 and *F*41, two pairs of interaction friction between *U*2 and the clamp plate *F*25 and *F*52, *F*26 and *F*62, and a pair of interaction friction between *U*1 and *U*2, *F*12 and *F*21. The pretightening forces of the two clips are *P*1 and *P*2, respectively.

2.2.2. Force Analysis of Lap Section after Clamp Pretightening. Assuming that the *U*-shaped steel in *U*2 section is fixed and the *U*-shaped steel in *U*1 section moves along the positive direction of the *Y*-axis due to the action of external load, *U*1 is taken as the analysis object for force analysis. After the clamp is pretightened, the external force on *U*1 includes the positive pressures *F*31 and *F*41 of the *L*3 and *L*4 bolts on *U*1 and the positive pressure *F*21 of the *U*2 on *U*1. At this time, the force balance equation for *U*1 is as follows:

$$\begin{aligned} F_{21} &= F_{31} + F_{41}, \\ F_{31} &= P_1 = \frac{M_1}{kd}, \\ F_{41} &= P_2 = \frac{M_2}{kd}. \end{aligned} \tag{1}$$

2.2.3. Force Analysis of Lap Section under Axial Load

(1) There is No Relative Sliding Axial Load between the Two U-Shaped Steels. In the initial stage of loading, the friction between the contact surfaces of the two *U*-shaped steels is greater than the axial load; there is no sliding friction between the *U*-shaped steels, and the clamp does not exhibit tilt deformation. At this stage, *U*1 is not only subjected to the positive pressure of *L*3 and *L*4 bolts and *U*2, but also subjected to the friction of *U*2 on *U*1. The balance equation of *U*-shaped steel in the *U*1 section is as follows:

$$\begin{aligned} \frac{p}{2} &= f_{21}, \\ F_{21} &= F_{31} + F_{41}, \\ F_{31} &= P_1 = \frac{M_1}{kd}, \\ F_{41} &= P_2 = \frac{M_2}{kd}, \end{aligned} \tag{2}$$

*U*1 does not slip, and the maximum axial load *P* is

$$p = 2f_{21} = 2\mu_1 F_{21} = 2\mu_1 (F_{31} + F_{41}). \tag{3}$$

(2) There is a Relative Sliding Stage between Two U-Shaped Steels. With the increasing of axial load, when the axial load is greater than the static friction force *f*21 between the *U*-

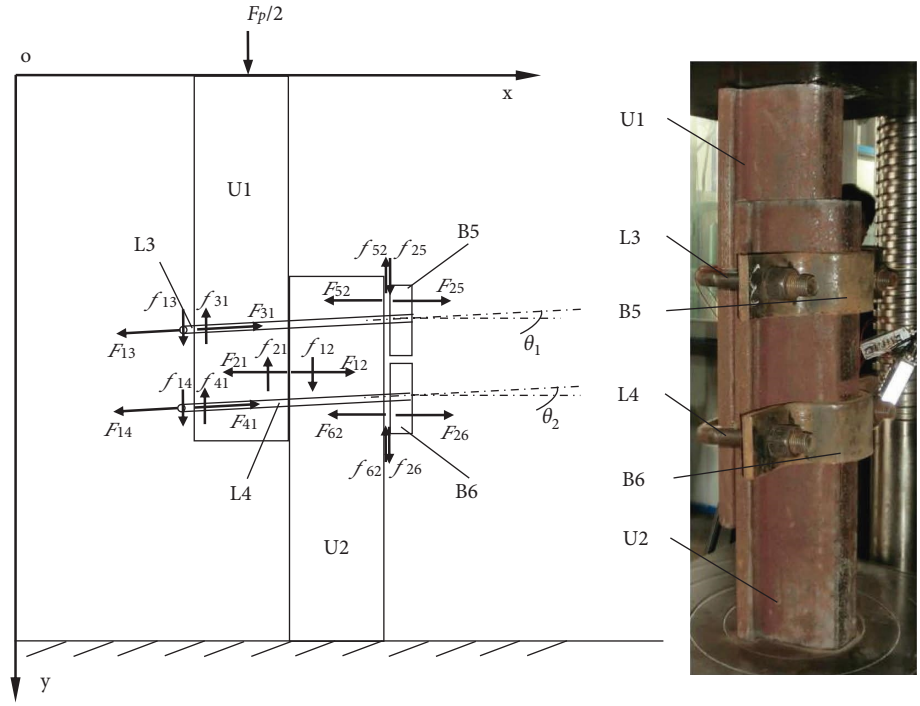

Figure 5: *U*-shape calculation model figure.

section steel, the relative sliding between the *U*-section steel *U*2 and the splint *B*5, *B*6 does not occur (the experiment found that during the sliding process of the *U*-section steel, the relative sliding between the splint and the *U*-section steel basically does not occur). Due to friction between *L*3 and *L*4 bolts and *U*1, *L*3 and *L*4 begin to tilt deformation. In this process, the balance equation for *U*1 steel is as follows:

$$\begin{aligned} F_{21} &= F_{31}\cos\theta_1 + F_{41}\cos\theta_2, \\ \frac{p}{2} &= f_{21} + f_{31} + f_{41} = \mu_1' F_{21} + f_{31} + f_{41}, \\ F_{31}\cos\theta_1 &= P_1 = \frac{M_1}{kd}, \\ F_{41}\cos\theta_2 &= P_2 = \frac{M_2}{kd}. \end{aligned} \tag{4}$$

*L*3, *L*4, and *U*1 do not slip, and the maximum axial load *P* is

$$p = 2\left(f_{21} + f_{31} + f_{41}\right) = 2\left(\mu_1' F_{21} + f_{31} + f_{41}\right). \tag{5}$$

Among them,

$$\begin{aligned} f_{31} &= \mu_1 F_{31}\cos\theta_1 = \mu_1 P_1, \\ f_{41} &= \mu_1 F_{14}\cos\theta_2 = \mu_1 P_2. \end{aligned} \tag{6}$$

From the abovementioned analysis, it can be seen that the friction between the bolt and the *U*-shaped steel causes tilt deformation of the bolt and generates additional stress inside the bolt. When the tilt reaches the maximum angle θ max, the bolt no longer tilts, and the relative sliding between the bolt and *U*-shaped steel begins. Since the sliding friction is less than the maximum static friction force, the sliding friction force is not enough to keep the original tilt deformation state of the bolt, so the clamp, under the action of internal force, is instantly restored to the state before the tilt, and the friction force between the bolt and *U*-shaped steel is sharply reduced, causing a sudden drop in the axial bearing capacity. Due to the nonuniform bolt material, geometric error in the processing process, uneven roughness of the *U*-shaped steel surface, and other factors, the two clings in the lap section may not be deformed and sliding at the same time; that is, the change law of friction force *F*13 and *F*14 may be inconsistent.

For *O*-shed support, in the support stage before sliding shrinkage, the internal force of *O*-shed support increases with the increase in surrounding rock confining pressure. When the axial internal force of the *O*-shed support is greater than the maximum axial load $F_{p\max 2}$ at the joint, there will be relative sliding between the beams at the joint, and the *O*-shed support begins to shrink and relieve pressure. $F_{p\max 2}$ determines the initial sliding resistance of *O*-shed support. In the process of *O*-shed support shrinkage, the friction force at the joint changes from static friction force to dynamic friction force. Because the dynamic friction force is less than the static friction force, this process will lead to a sudden reduction in the bearing capacity of the support. The surrounding rock-support resistance will also suddenly decrease, which will have an impact on the support and cause damage to it. During the continuous shrinkage of *O*-shed support, plastic deformation will occur due to the constant friction between the brackets and the section steel, which may lead to a change in the friction properties between the brackets and the section steel, resulting in the failure of the brackets to work at the same time.

3. Deformation and Failure Analysis of *U*-Section Steel under Impact Load

3.1. Model Establishment and Parameter Selection. Taking *O*-shaped shed support (closed round *U*-shaped steel support) as the research object, the numerical simulation analysis of *U*-shaped steel support deformation under impact load was carried out. In order to reduce the calculation amount, a half-semicircular arch model was established for numerical simulation analysis. The *U*-shaped steel support is 36-*U* steel, the radius of the support is 3 m, and symmetrical constraints about the *Z* direction are adopted for the ends of the semicircular arch. The section and model of the section steel are shown in Figure 6; the constraints, action position, and loading direction of the impact plate are shown in Figure 7. The bearing capacity of the *U*-shaped steel support is tested by monitoring the reaction force of the impact plate when it is supported. The loading mode of clamp preload is shown in Figure 8. The clamp preload torque is 250 Nm, which is converted to 65 MPa of pressure applied on the nut surface. The analysis steps are divided into two steps. The first step is to load the clamping preload, and the second step is to use the rigid plate to impact the *U*-shaped steel support. The impact speed of the steel plate is 10 m/s, and the impact time is 0.04 s. *U*-shaped steel and clip material parameters are shown in Table 1. The friction coefficient between contact surfaces is 0.35.

3.2. Influence of Impact Load Form on Deformation and Failure of U-Shaped Steel. In order to study the influence of the impact load form on the stress and deformation of the *U*-shaped steel support, the stress and deformation of the support are simulated, respectively when the impact source is close to the support in the form of a concentrated load and when the impact source is far from the roadway in the form of a uniform load.

3.2.1. Stress and Deformation of U-Section Steel Support under Concentrated Load Impact. The bearing capacity variation curve of the *U*-section steel support under concentrated load impact is shown in Figure 9. As can be seen from the figure, the bearing capacity of the support fluctuates during the impact of the impact plate on the support. When the displacement of the impact plate is less than 200 mm, the bearing capacity of the support basically remains above 250 kN; when the displacement of the impact plate exceeds 200 mm, the bearing capacity of the support decreases rapidly.

When $t = 0.028$ s, the bearing capacity of the support is 263 kN, the displacement of the impact plate on the support is 241 mm, and the sliding distance of the joint is 120 mm. The stress and displacement of the *U*-shaped steel support are shown in Figure 10. At this time, the section steel support at the impact point of the support by the impact plate has undergone serious buckling deformation, and the stress at some positions has exceeded the strength limit of the support material. The steel bracket has been destroyed; the stress in most positions of the steel bracket near the joint exceeds the yield strength, and the high-stress concentration area appears in individual positions of the clamp splint, but it does not exceed the yield limit of the clamp material.

3.2.2. The Impact of Uniformly Distributed Load; the Stress and Deformation of U-Shape Set under the Uniform Load Impact. The bearing capacity curve of the *U*-shape set as shown in Figure 11 can be seen from the diagram. The shock plate in the process of stents causes fluctuations in bearing capacity; the extreme value increases gradually, but overall capacity is mainly because the impact plate at each load point supports the load at the same time. Each component of the support also interacts with each other to make the support shrink, and the reaction force of the impact plate decreases rapidly because the loading speed of each loading point cannot keep up with the contraction speed of the support.

When $t = 0.028$ s, the stress and displacement of the *U*-shaped steel support are shown in Figure 12. At this time, the bearing capacity of the support is 276 kN, the displacement of the impact plate acting on the support is 262 mm, and the sliding distance of the joint is 523 mm. The internal force of the whole support is evenly distributed, and the stress at most positions of the section steel exceeds the yield strength. The support has entered the plastic state, the local stress on the clamp is high, and the stress at some points exceeds the yield strength.

Through the abovementioned simulation results, it can be seen that the uniformly distributed load type *O* tents stent bearing capacity and energy absorption is better than the following load type *O* tents stent, a single lap joint section of energy absorption can promote more than 4 times, so the impact ground pressure type *O* shed between supports and surrounding rock of roadway should increase the filling layer, increase *O* shed the coupling of supports and surrounding rock.

4. Failure Characteristics Analysis and Optimization Scheme of *U*-Section Steel in Rock Burst Roadway

4.1. Failure Characteristics Analysis of U-Section Steel. Through the research on the impact ground pressure characteristics of roadway support, it was found that *U*-shaped steel stents can provide effective support to the crushed surrounding rock of the roadway, but their use in an impact ground pressure tunnel causes local bending failures and phenomena such as buckling deformation damage that make the bearing capacity of the *U*-shape set far less than the design value. Combining the working principle of the *u*-shape set with the experiment and theoretical analysis, it is found that the failure characteristics of the *U*-shaped steel support in deep rock burst roadways mainly have two forms.

4.1.1. Overall Instability Failure of the Support. Impact of deep roadway surrounding rock pressure, impact pressure release energy level is bigger, roadway supporting parameters design is unreasonable, if the effect on the *U* steel support of surrounding rock pressure is more than the load

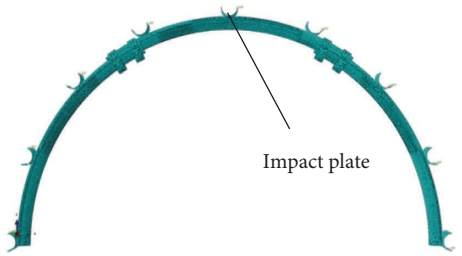

Figure 6: Calculation model figure of *U*-shaped steel bracket.

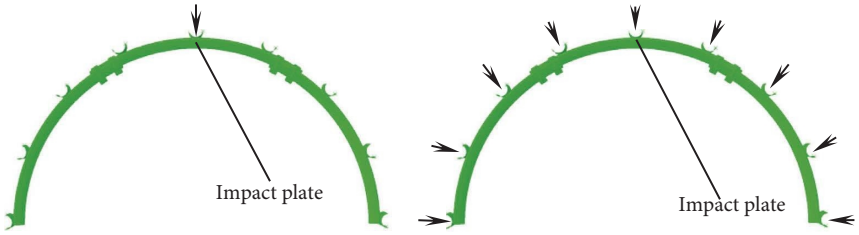

Figure 7: Loading method and measuring point. (a) Concentrated load action and (b) uniform load action.

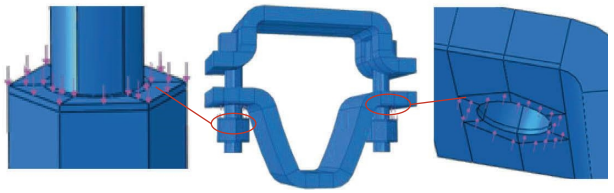

Figure 8: Pretightening force loading method of clamp.

Table 1: *U*-shaped steel and card material parameters.

	Density (kg/m^3)	Elastic modulus (GPa)	Poisson's ratio	Yield strength (MPa)	Tensile strength (MPa)	Ultimate strain (%)
U-shaped steel	7800	210	0.31	270	530	20
Clamps	7800	210	0.3	720	908	18

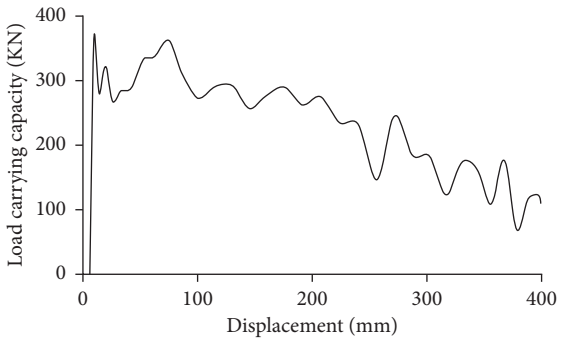

Figure 9: Bearing capacity changing curve of retractable *O*-shed stent under concentrated impact loading.

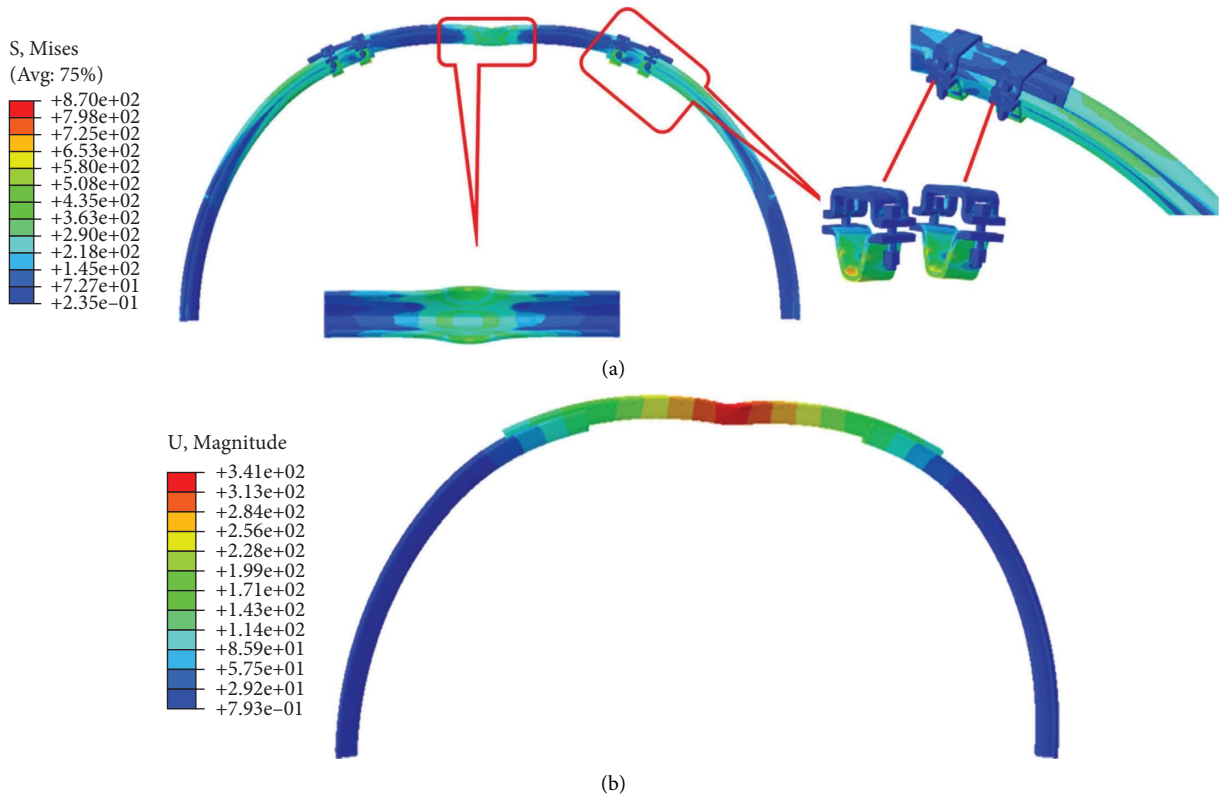

Figure 10: Stress and displacement nephogram of the stent ($t = 0.028$ s). (a) Support stress and deformation diagram. (b) Support the displacement and deformation diagram.

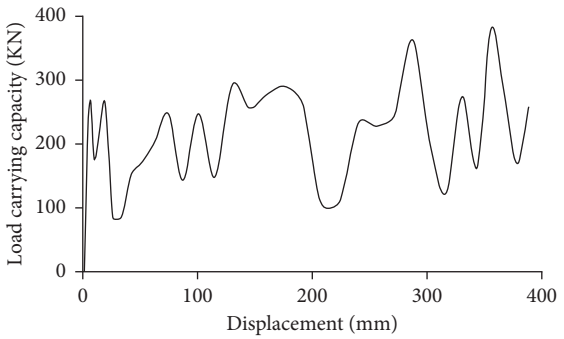

Figure 11: Bearing capacity changing curve of retractable *O*-shed stent under uniform impact loading.

limit, it causes the framework as whole or partial damage, such as individual steel stent bend, part of the card pull rod fracture, fracture, falling back, waiting for a phenomenon. The inclined, bent, and even broken surrounding supports were induced, and then the instability of the whole support was induced. The section size and structural characteristics of the *U*-shaped steel support determine its limited bearing capacity, and its main role is to maintain the stability of coal and rock masses in the broken area of the roadway. For a deep, high-stress roadway, *U*-shaped steel support needs to be combined with bolts, anchor cables, and hydraulic support to form three-level anti-impact support.

4.1.2. Failure and Destruction of Bracket Lap Segment. The main feature of the *U*-shaped steel support is that the lap segment can shrink smoothly and maintain constant support resistance, so the sliding shrinkage performance of the lap segment has a very important influence on the support performance. The failure characteristics of a large number of *U*-shaped steel supports in deep rock burst roadways show that the supporting resistance of *U*-shaped steel supports will drop suddenly or the support will shrink when the clamping force is insufficient, the clamping bolt is broken, and the joint is killed. Then, the lap section is damaged, and the anti-impact performance is seriously affected. Therefore,

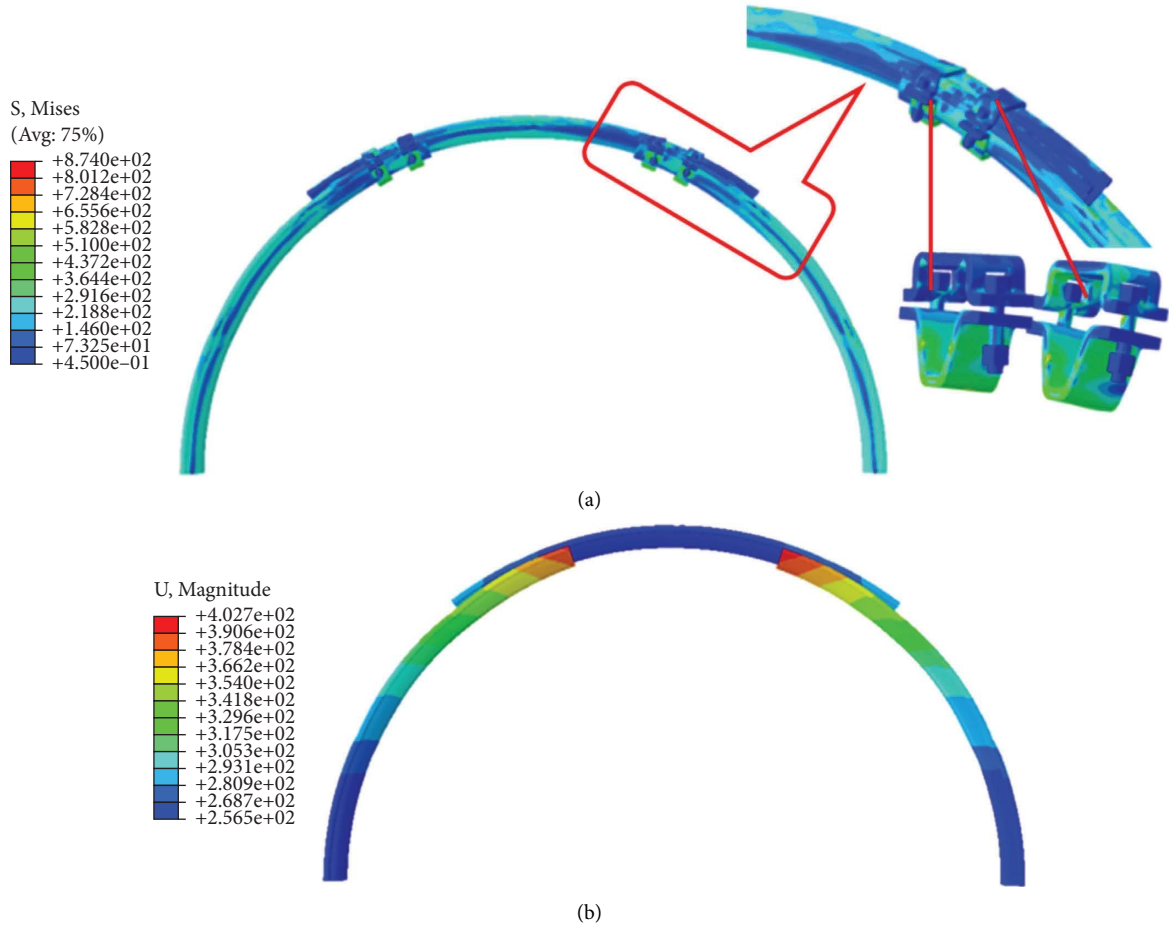

Figure 12: Stress and displacement nephogram of the stent ($t = 0.028$ s). (a) Support stress and deformation diagram. (b) Support the displacement and deformation diagram.

improving the sliding characteristics of the lap section is the key to improving the overall bearing capacity and impact resistance of *U*-shaped steel supports.

4.2. Optimization of Sliding Performance of U-Section Steel Lap Section. Through the abovementioned analysis, it can be seen that due to the hard-hard contact between the *U*-shaped steel and the clamp, the discontinuity and inhomogeneity of the contact surface determine that the friction force cannot change stably in the process of shrinkage and sliding, resulting in the stress drop of the clamp screw and the increase of shear force, resulting in the loosening of the clamp or the fracture of the screw. In order to ensure the stability of the friction between the *U*-shaped steel and the bolt, a layer of soft gasket can be added between the *U*-shaped steel and the bolt contact surface to change it into hard-soft contact, so that the contact between the friction surfaces becomes closer and the friction performance of the contact surface is improved [34].

Figure 13 shows the axial load-displacement curve of the lap section after adding a cushion between the *U*-shaped steel and the contact surface of the bolt. As can be seen from the figure, the change in axial bearing capacity is relatively stable, and there is no sudden drop in bearing capacity.

Figure 14 shows the change in the curve of the bolt's internal force when a soft gasket is added between the clamp *U*-bolt and *U*-shaped steel. It can be seen from the figure that, in the process of the contraction of the lap segment, the internal forces of the bolts at the three measuring points of the upper and lower clamps all changed stably without a sudden drop.

It can be seen that adding a cushioned plate between the bolt and the *U*-shaped steel can effectively improve the contact conditions between the *U*-shaped steel and the bolt, avoid the instantaneous large displacement sliding of the bolt, ensure the stable change of the bearing capacity, make the two clamps work effectively at the same time, prevent the clamps from pretightening and loosening, enhance the pretightening effect, and ensure the stable change of the bearing capacity of the joint during the contraction of the *U*-shaped steel bracket. There is no sudden drop phenomenon, which makes the support resistance of the *U*-shaped steel bracket stable during the process of shrinkage, and it increases the friction energy absorption of the joint during the process of shrinkage.

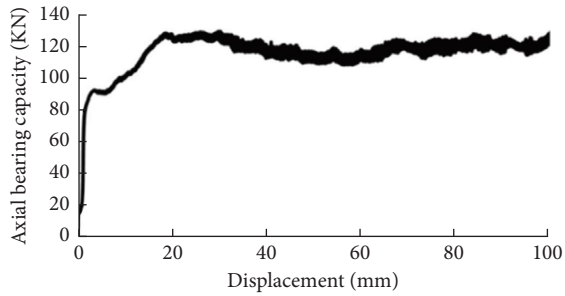

Figure 13: Axial load-displacement relation curve of a *U*-type steel lap joint.

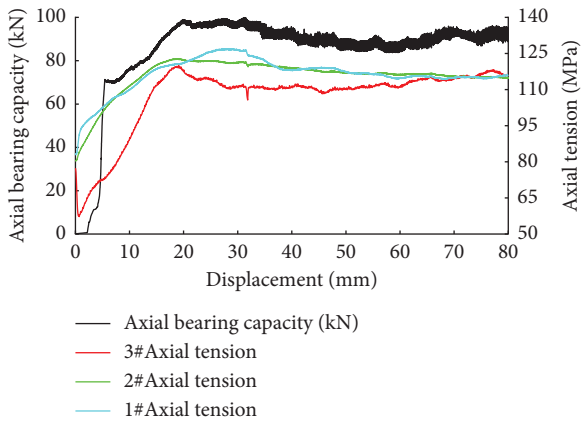

Figure 14: The change in the curve of the internal force of the bolt when adding a rubber gasket.

5. *O*-Type Shed Design and Field Application for Rock Burst Roadway Stability and Constant Resistance Energy Absorption

5.1. Basic Design Idea of O-Type Stable Structure Constant Resistance Energy Absorption Shed. Based on the occurrence mechanism of roadway rock burst, the propagation and attenuation law of impact stress wave, the working principle of *O*-type shed support, and the energy absorption and anti-impact support mechanism, the structural design of stable and constant resistance energy absorption *O*-type shed support should meet the following three requirements: (1) *O*-type shed support must have a high bearing capacity, maintain the usual surrounding rock static load pressure, but also have the impact resistance of shrinkage deformation and maintain the bearing capacity. It must also timely reduce the impact of the *O*-type shed support stress level and maintain the overall stability and bearing capacity of the *O*-type shed structure; (2) *O*-type shed support and its wall filling should have high impact resistance to alleviate the impact of surrounding rock on the *O*-type shed support; (3) the surrounding rock-support structure forms a holistic support structure that makes full use of the characteristics of broken coal rock, the damping of surrounding rock, and the wave impedance between layers of structures with different strengths to absorb and dissipate the impact energy so that the impact stress wave transmitted through the surrounding rock rapidly attenuates [35] and greatly improves the stability and impact failure resistance of the surrounding rock-support structure.

5.2. Steady Structure Constant Resistance Energy Absorption O-Type Shed Design. Stable constant resistance energy absorption *O*-type shed support structure, mainly including stable constant resistance energy absorption *O*-type shed support, energy absorption buffer filling layer behind the wall, energy absorption and shock absorption partition surrounding rock, etc.

5.2.1. Stable Constant Resistance Energy Absorption O-Type Shed Support. According to the abovementioned studies, in order to improve the shrinkage deformation ability and bearing capacity stability of the *O*-shed support, gaskets can be added between the section steel at the joint and the contact surface of the clamp, as shown in Figure 15, to improve the rapid shrinkage performance and energy absorption of the support joint. The good shrinkage performance of the support joint can provide space for the surrounding rock's deformation and transform the impact kinetic energy into the surrounding rock's internal energy and other energies. To avoid the strength damage caused by the bearing capacity of the bracket exceeding the bearing limit, this paper adopted the addition of gaskets between the joint steel and the contact surface of the clamp to change the sliding friction performance between the contact surface, improve the rapid shrinkage performance and energy absorption of the bracket, and enhance the energy absorption and anti-impact performance of the *O*-shaped shed bracket. The sliding friction performance between contact surfaces was changed to improve the rapid shrinkage performance and energy absorption of the support, and the bearing capacity of the *O*-shaped shed support was stably changed.

5.2.2. Energy Absorption Buffer Wall after Filling. In order to enhance the coupling degree between the support and surrounding rock and the energy absorption buffer effect under impact conditions, wood and other fillers with energy absorption buffer function are filled between the support and coal wall. In the period of roadway without rock burst, the coupling degree of support and surrounding rock is increased, so that the support is evenly loaded and the bearing capacity is improved. When a rock burst occurs, the backwall filling deformation is used to absorb the impact energy, increase the time of impact load acting on the support, reduce the peak impact load acting on the support, and prevent the support from overload damage.

5.2.3. Surrounding Rock with Energy Absorption and Shock Absorption. Through grouting anchorage, hydraulic slotting, deep hole blasting, and other technologies, the surrounding rock is formed into zoned surrounding rock with a multilayer fracture zone. The impact stress wave can be reflected by the interface of coal and rock with different physical and mechanical properties in the surrounding rock, and the impact pressure on the support can be greatly

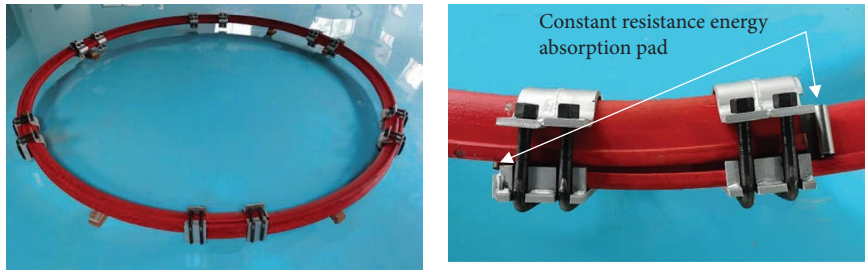

(a) (b)

Figure 15: The physical picture of the stable structure is constant resistance energy absorption in an"O" type shed. (a) The overall picture. (b) An enlarged view of the lap and the curved constant resistance pad.

reduced. By increasing the plastic zone thickness of the surrounding rock, the energy absorption of the surrounding rock can be improved by using the energy absorption and shock absorption performance of low-strength broken coal and rock mass, and the vibration frequency and amplitude of the support can be greatly reduced in the process of impact. The anti-impact and shock absorption performance of the surrounding rock can also be improved.

5.3. Field Application. A field test of *O*-type stable constant resistance energy absorption was carried out in the 63007# return air roadway of Laohutai Mine, as shown in Figure 16. Before mining, the coal seam is softened by water injection, which reduces the strength of the coal seam. The surrounding rock of the roadway wall is anchored by bolts, which increases the residual strength of the surrounding rock near the roadway. Between the roadway and surrounding rock, wood with better buffer performance is used as filling material, and the coupling degree between the surrounding rock and *O*-type shed support is higher.

In order to detect the supporting effect of a stable constant resistance energy absorption *O*-type shed, the slip momentum of the joint of the stable constant resistance energy absorption *O*-type shed, the relative movement of the roof and floor, the relative movement of the two sides, and the deformation and damage of the stable constant resistance energy absorption *O*-type shed were monitored, respectively. The detection location is shown in Figure 17. In the figure, *l*1 is the relative movement of the roof and floor; *l*2 is the relative movement of two sides; and *D*1, *D*2, *D*3, and *D*4 are the slip momentum of the *O*-type shed support joint.

During the monitoring period, 5 shock events occurred near the working face. The impact events are mainly located on the roof and floor of the working face, and the impact source is within the range of 50–120 m from the roadway. They are mainly rock bursts with low energy and below medium level, and two of them are moderate impact events (Days 9 and 19).

5.3.1. Relative Displacement of Surrounding Rock of Roadway. Under the influence of working face mining, the surrounding rock of the roadway gradually deforms as the working face moves forward, and the relative proximity between the roof and floor and the two sides gradually increases. As shown in Figure 18, the maximum relative proximity between the roof and floor of the roadway at # 2 increases by about 30 mm and 200 mm, respectively, due to the two medium-impact events. The relative proximity between the two sides increases by about 20 mm and 200 mm, respectively. The surrounding rock of the roadway is stable despite deformation. The other three impact events are small energy impact events with a low impact. Under the *U*-shaped steel support, the surrounding rock of the roadway hardly has much deformation. According to the previous experience of the mine, moderate impact events usually cause serious deformation and failure of the surrounding rock of the roadway, and part of the coal rock bursts into the roadway, while the stability of the control surrounding rock is significantly enhanced by the optimized *U*-shaped steel bracket.

5.3.2. Sliding Displacement and Deformation Failure at the Lap Joint of U-Shaped Steel Support. After completion of the erection of the *U*-shape set, due to the passive support for the *U*-shape set, a timely *U*-shape set effective load cannot be achieved. The rock under the anchorage force of the bolt and the relative stability of the surrounding rock caused slow deformation, gradually extrusion, *U*-shape set with the increase of time, and the surrounding rock pressure of *O*-shed increased gradually. When the weak impact event occurs, the residual strength of coal and rock in the anchoring area of the roadway surrounding the rock is large, and no large deformation occurs in the anchoring area, and no large impact pressure is formed on the *U*-shaped steel support. In the two moderate impact events, the *U*-shaped steel support obviously contracted. However, *U*-shaped steel has no obvious bending, buckling, or other phenomena, which can well control the surrounding rock deformation of the roadway. According to the previous experience of the mine, moderate impact events usually cause obvious bending deformation and clamping loosening failure at the joints of *U*-shaped steel supports, and obvious lateral bending and buckling deformation will occur in local parts of *U*-shaped steel supports, so *U*-shaped steel supports need to be replaced and repaired. This is mainly because, after the increase in the plate, the sliding performance of the *U*-shaped steel support joint is better. When the impact occurs, the resistance of the

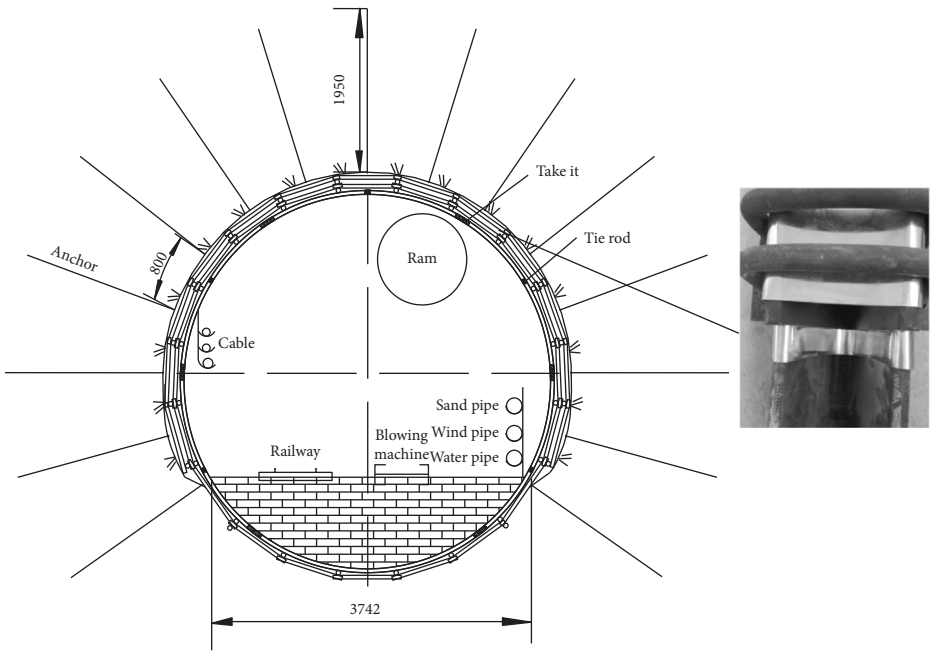

Figure 16: Schematic diagrams of stable structure and constant resistance energy absorption *O*-shed.

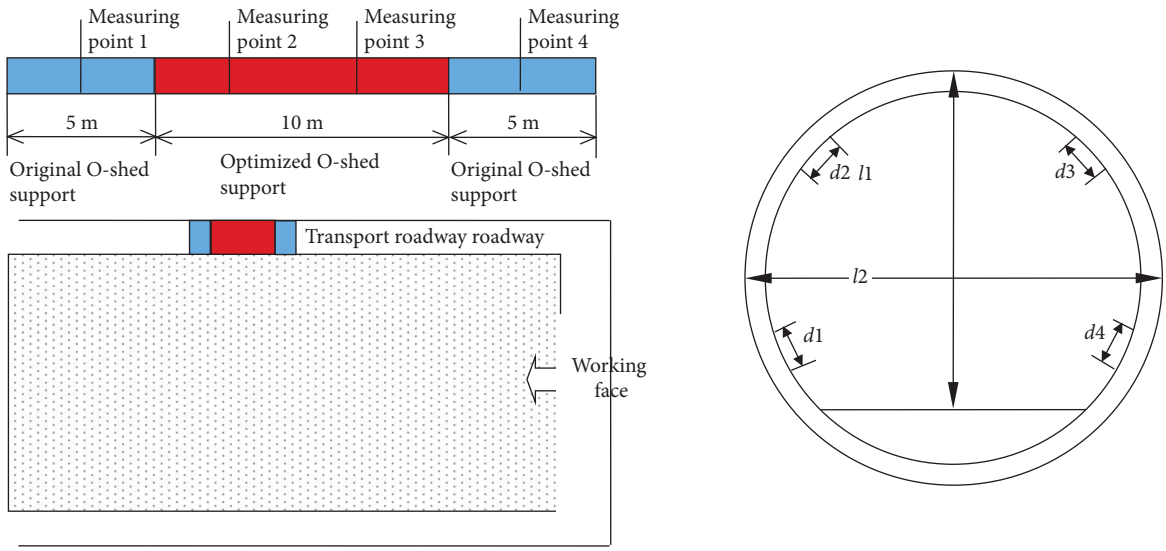

Figure 17: Layout of monitoring points.

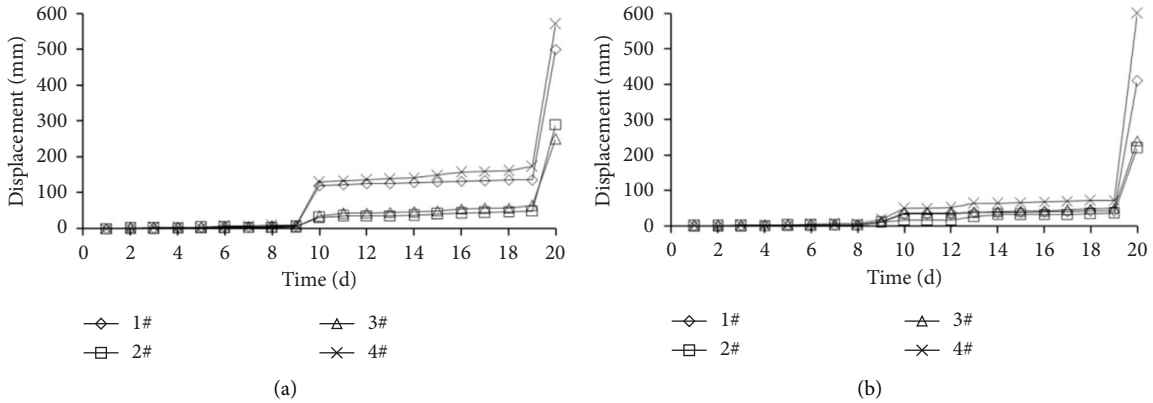

Figure 18: Variation curve of the roadway surrounding rock over time. (a) Displacement of the top and bottom plates; (b) displacement of two sides.

U-shaped steel support is high and timely contraction occurs, and the phenomenon of slip-resisting and low-resistance contraction will not occur, so that the overall stability of the *U*-shaped steel support and the ability to resist side impact are improved.

6. Conclusion

(1) Through the slip experiment of the lap section, the slip mechanism of the lap section is analyzed, and it is found that adding a soft gasket between the screw and *U*-section steel can increase the friction coefficient between the screw and *U*-section steel, improve the properties of the contact surface between the screw and *U*-section steel, increase the energy absorption in the process of shrinkage, avoid the sudden drop in axial bearing capacity, and prevent the uneven force of clamp. The support resistance and energy absorption of the *U*-shaped steel bracket can be effectively improved, and the anti-impact performance of the roadway supporting structure can be improved.

(2) The stress and deformation characteristics of the *U*-shaped steel support under concentrated impact load and uniform impact load are analyzed. From the numerical simulation results, it can be seen that the load-bearing performance and energy absorption of the *U*-shaped steel support with a uniform load are better than those of the *U*-shaped steel support with a centralized load.

(3) A stable *O*-type shed structure with constant resistance and energy absorption is proposed. In the field application, it is found that the original *U*-shaped steel supports can resist the rock burst below the middle grade with a low impact damage degree, and some *U*-shaped steel supports will be deformed, but the surrounding rock of the roadway is basically stable. For the medium-grade rock burst with a high degree of impact damage, the original *U*-shaped steel support is severely deformed and damaged and cannot maintain the stability of the roadway surrounding the rock after the impact. However, the newly designed *U*-shaped steel support has a higher bearing capacity, better shrinkage, and deformation performance, and still has higher support resistance after the impact.

Data Availability

The data used to support the findings of this study are included within the article.

Conflicts of Interest

The authors declare that they have no conflicts of interest.

Acknowledgments

This work was supported by the National Natural Science Foundation of China (U1908222), National Natural Science Foundation of China (51904141), and National Basic Research Program of China (2017YFC0804205).

References

[1] L. Xu, *Research on the Prevention and Control Rock Burst of O Shed Support in the Roadway*, Liaoning Technical University, Fuxin, China, 2016.

[2] J. Zhou, D. Li, and D. Li, "Application of high-strength *u*-shaped steel support in soft rock roadway support," *Coal Technology*, vol. 25, no. 12, 2010.

[3] H. Kang, J. Lin, and M. J. Fan, "Investigation on support pattern of a coal mine roadway within soft rocks a case study," *International Journal of Coal Geology*, vol. 140, pp. 31–40, 2015.

[4] Le Yang, C. You, and Y. Zhao, "Mechanical analysis of collapsible supports for roadway grille," *Journal of China Coal Society*, vol. 40, no. 10, pp. 2484–2489, 2015.

[5] X. Tan, W. Chen, and H. Liu, "A combined supporting system based on foamed concrete and *U*-shaped steel for underground coal mine roadways undergoing large deformations," *Tunnelling and Underground Space Technology incorporating Trenchless Technology Research*, vol. 68, 2017.

[6] Y. Zhao, Na Liu, X. Zheng, and N. Zhang, "Mechanical model for controlling floor heave in deep roadways with *U*-shaped steel closed support," *International Journal of Mining Science and Technology*, vol. 25, no. 5, pp. 713–720, 2015.

[7] Y. Wu, J. Chen, and J. Jiao, "Damage and failure mechanism of anchored surrounding rock with impact loading," *Journal of China Coal Society*, vol. 43, no. 09, pp. 27–35, 2018.

[8] *Yishan Pan Coal Mine Impact Ground Pressure*, pp. 575-576, Science Press, Beijing, China, 2018.

[9] Q. Qi, Y. Pan, and L. Shu, "Theory and technical framework of prevention and control with different sources in multi-scales for coal and rock dynamic disasters in deep mining of coal mines," *Journal of China Coal Society*, vol. 43, no. 07, pp. 1801–1810, 2018.

[10] C. Wang, M. Wang, S. Gong, J. Zou, and K. Wu, "Study on evolution law and the mechanical mechanism of strong mine tremors in a deep coal mine," *Advances in Civil Engineering*, vol. 202210 pages, Article ID 1066833, 2022.

[11] R. Cao, P. Cao, and H. Lin, "Support technology of deep roadway under high stress and its application," *International Journal of Mining Science and Technology*, vol. 26, no. 5, pp. 787–793, 2016.

[12] J. Wang, Y. Zuo, and L. Dong, "Optimization of *u*-shaped steel support for deep roadway in complex geological mines," *China Safety Science Journal*, vol. 28, no. 12, pp. 100–105, 2018.

[13] H. Wang, P. Zheng, W. Zhao, and Hm Tian, "Application of a combined supporting technology with *U*-shaped steel support and anchor-grouting to surrounding soft rock reinforcement in roadway," *Journal of Central South University*, vol. 25, no. 5, pp. 1240–1250, 2018.

[14] L. Jing, Q. Jiang, and N. Liu, "Numerical simulation and analysis of *u*-shaped steel support in roadway of extremely loose coal seam," *Coal Mining Technology*, vol. 17, no. 6, pp. 48–51, 2012.

[15] W. Xie, Q. Wang, and S. Jing, "Supporting mechanism and bearing law of *u*-shaped steel brace-anchor cable combined support under dynamic pressure in roadway," *Journal of China Coal Society*, vol. 40, no. 02, pp. 301–307, 2015.

[16] J. Liang, L. Huang, J. Ma, and W. Chen, "A dynamic bounding surface plasticity damage model for rocks subjected to high

strain rates and confinements," *International Journal of Impact Engineering*, vol. 168, Article ID 104306, 2022.

[17] J. Ma, J. Chen, J. Guan, Y. Lin, W. Chen, and L. Huang, "Implementation of Johnson-Holmquist-Beissel model in four-dimensional lattice spring model and its application in projectile penetration," *International Journal of Impact Engineering*, vol. 170, Article ID 104340, 2022.

[18] J. Ma, J. Chen, W. Chen, and L. Huang, "A coupled thermal-elastic-plastic-damage model for concrete subjected to dynamic loading," *International Journal of Plasticity*, vol. 153, Article ID 103279, 2022.

[19] W. Xie, S. Jing, and T. Wang, "Structural stability and control technology of *u*-shaped steel supports," *Chinese Journal of Rock Mechanics and Engineering*, vol. 29, no. 2, pp. 3743–3748, 2010.

[20] J. Wang, Ke Yang, and P. Zhu, "Buckling deformation and instability analysis of *u*-shaped steel support in deep rock roadway," *Mining Safety & Environmental Protection*, vol. 45, no. 01, pp. 98–106, 2018.

[21] L. Huang, J. Ma, M. Lei, L. Liu, Y. Lin, and Z. Zhang, "Soil-water inrush induced shield tunnel lining damage and its stabilization: a case study," *Tunnelling and Underground Space Technology*, vol. 97, Article ID 103290, 2020.

[22] L. Huang, J. Liang, J. Ma, H. Yang, and Y. Gui, "Spherical cavity expansion in porous rock considering plasticity and damage," *International Journal for Numerical and Analytical Methods in Geomechanics*, vol. 45, no. 15, pp. 2235–2259, 2021.

[23] Y. Jiao, L. Song, X. Wang, and A. Coffi Adoko, "Improvement of the *U*-shaped steel sets for supporting the roadways in loose thick coal seam," *International Journal of Rock Mechanics and Mining Sciences*, vol. 60, pp. 19–25, 2013.

[24] Z. Ma, Y. Jiang, and Y. Li, "Collaborative control of borehole pressure relief and *u*-shaped steel in extremely soft coal seam," *Journal of China Coal Society*, vol. 40, no. 10, pp. 2279–2286, 2015.

[25] C. You, "Shrinkage analysis of yielding support of *u*-shaped steel," *Journal of China Coal Society*, vol. 19, no. 03, pp. 270–277, 1994.

[26] J. Ma, J. Guan, Y. Gui, and L. Huang, "Anisotropic bounding surface plasticity modelfor porous media," *International Journal of Geomechanics*, vol. 21, no. 4, Article ID 04021033, 2021.

[27] Y. Chen and W. Mao, "The prediction of cracking load and peak load of UHPC-NC composite structure," *Advances in Civil Engineering*, vol. 2022, pp. 1–12, 2022.

[28] X. Zeng, *Study on Stress Characteristics and Deformation Failure of U-Shaped Steel Support in Rock Burst Roadway*, Liaoning Technical University, Fuxin, China, 2015.

[29] X. Li, C. Wang, H. Wang, and Bo Diao, "Experimental study on bearing characteristics of *u*-shaped steel enclosed and collapsible steel frame," *Journal of Zhejiang University*, vol. 51, no. 12, pp. 2355–2364, 2017.

[30] J. Liu, Z. X. Z. Nong, and B. Wang, "Analysis of longitudinal stress and buckling failure of *u*-shaped steel supports," *Journal of China Coal Society*, vol. 36, no. 10, pp. 1647–1652, 2011.

[31] Y. Zhang and C. Hou, "Calculation of the actual bearing capacity of *U*-shaped steel retractable roadway bracket," *Mine Pressure and Roof Management*, vol. 3, no. 03, pp. 16–22, 1992.

[32] S. Yao and Z. Du, "Mechanical calculation and analysis of *U*-shaped steel retractable bracket card cable," *Coal Science and Technology*, vol. 13, no. 04, pp. 40–44, 1985.

[33] C. Wang, N. Zhang, and C. Han, "Numerical analysis and application of the relationship between *u*-shaped frame lock leg support and surrounding rock," *J Journal of Mining & Safety Engineering*, vol. 28, no. 2, pp. 209–213, 2011.

[34] L. Xu, Y. Pan, and J. Chen, "Experimental study on friction properties and optimization of *u*-shaped steel bracket joints," *Journal of China Coal Society*, vol. 43, no. 11, pp. 2992–2998, 2008.

[35] L. Xu, Y. Pan, and X. Zeng, "Study on the energy-absorbing cushion performance of roadway surrounding rock crushing zone[J]," *Journal of China Coal Society*, vol. 40, no. 06, pp. 1376–1382, 2015.